Weakly and strongly coupled Belousov-Zhabotinsky patterns

Stephan Weiss[1,*] and Robert D. Deegan[2,†]
[1]*Max Planck Institute for Dynamics and Self-Organization (MPIDS), 37077 Göttingen, Germany*
[2]*Center for the Study of Complex Systems, University of Michigan, Ann Arbor, Michigan 48109, USA*
(Received 8 November 2016; published 24 February 2017)

We investigate experimentally and numerically the synchronization of two-dimensional spiral wave patterns in the Belousov-Zhabotinsky reaction due to point-to-point coupling of two separate domains. Different synchronization modalities appear depending on the coupling strength and the initial patterns in each domain. The behavior as a function of the coupling strength falls into two qualitatively different regimes. The *weakly coupled* regime is characterized by inter-domain interactions that distorted but do not break wave fronts. Under weak coupling, spiral cores are pushed around by wave fronts in the other domain, resulting in an effective interaction between cores in opposite domains. In the case where each domain initially contains a single spiral, the cores form a bound pair and orbit each other at quantized distances. When the starting patterns consist of multiple randomly positioned spiral cores, the number of cores decreases with time until all that remains are a few cores that are synchronized with a partner in the other domain. The *strongly coupled* regime is characterized by interdomain interactions that break wave fronts. As a result, the wave patterns in both domains become identical.

DOI: 10.1103/PhysRevE.95.022215

I. INTRODUCTION

The Belousov-Zhabotinsky (BZ) reaction is an oscillating chemical reaction wherein a catalyst periodically cycles between a reduced and an oxidized state. This cycling produces a periodic color change in a well-mixed solution [1–3] and spatiotemporal patterns, typified by spiral or target waves in two dimensions [2,4,5] and scroll waves in three dimensions [4,6], when the spatial extent of the reactants is limited by diffusion. The shape and dynamics of these patterns are characteristic of a broad class of oscillatory and excitable systems that includes heart tissue [7], chicken retina [8], human tongues [9], or colonies of starving amoeba [10]. Therefore, the BZ reaction is an important model system for investigating pattern formation in excitable and oscillatory media and has been extensively researched for many decades (see, for example, Refs. [5,11–14]).

A typical single-armed spiral wave (see Fig. 1) consists of a core and a spiral-shaped wave front whose innermost end—its tip—orbits the core. We define the spiral wave phase ψ as the angular position with respect to the vertical of the spiral tip on the core, as shown in Fig. 1. In time the spiral appears to rotate counterclockwise as the wave front propagates outward. Depending on the chemical concentration, the core is either stationary or mobile; in our system the core is stationary in the absence of coupling.

Using the ruthenium complex compound tris (bipyridyl) dichlororuthenium [$Ru(bpy)_3^{2+}$] as the catalyst, the reaction kinetics can be regulated by blue light ($\lambda_l \approx 450\,\mathrm{nm}$) [15]. In particular, the propagation speed of the wave front, and hence the rotation rate of the spiral, can increase or decrease depending on the light intensity and the concentration of the other reactants. In the more common case, illumination produces additional bromide ions (Br^-) that inhibit the reaction and decrease wave-front speeds and spiral rotation rates [16,17]. For large concentrations of sodium bromate ($NaBrO_3$), however, illumination was reported to increase the wave speed [16], and while the exact mechanism remains obscure, at these concentrations illumination induces the production of the activator $HBrO_2$ [18,19].

The *light-sensitive BZ reaction* is a convenient system for studying the behavior of spiral waves subjected to temporally periodic forcing. Zykov and coworkers conducted numerical and experimental observations of the spiral tip's motion due to periodic forcing at various frequencies and intensities [20,21]. In their unforced system, tips moved on simple circles around the core (i.e., rigid rotation). When exposed to periodic forcing, the tip traveled on an epicycloid with the large radii inversely proportional to the difference between the forcing frequency and the spiral frequency of the unforced system. Additional resonances and synchronization phenomena were found for spirals that exhibit epicycloidal motion in the unforced system. Mantel and Barkley developed a zero-dimensional coupled system of differential equations for the trajectories of periodically forced spirals using only the position of the cores as the dynamic variable [22]. Additional experiments showed that spirals forced with planar traveling waves move on straight trajectories [23].

In the above investigations the forcing strength, i.e., the light intensity was small, and so only the wave front speed was affected. Experiments by Lin and coworkers [13,17,24,25] showed that rotating spirals are destroyed when forced at sufficiently large strength. The spiral wave patterns are then replaced by oscillating domains with fixed boundaries that resonate with the applied forcing frequencies.

Grill *et al.* [26] measured the influence of feedback stimuli on spiral core motion. In their experiments and simulations, whenever a wave front reached a preselected trigger point on the spatial domain, a light pulse was applied to the core after a certain time delay. Depending on the time delay, the illumination intensity, and the distance between the trigger point and the spiral core, the core exhibited cycloidal motion very close to the trigger point (*entrainment attractor*) or larger circles around that point (*resonance attractor*).

*stephan.weiss@ds.mpg.de
†rddeegan@umich.edu

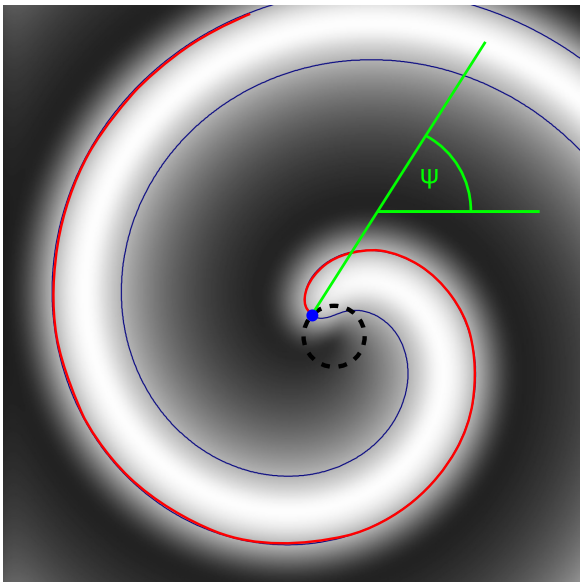

FIG. 1. The central region of a counterclockwise rotating spiral wave. The gray scale represents inhibitor concentration. The most salient features are the front of the wave (thick red line), the tail of the wave (blue thin line), the spiral tip (blue dot) where the front and tail meet, the core defined as the zone enclosed by the trajectory of the spiral tip (dashed circle), and the phase of the spiral ψ.

Hildebrand *et al.* [27] examined two weakly coupled BZ domains with the catalyst immobilized in a silica gel matrix. They projected the image of one reactor onto the other and vice versa. They showed that the patterns in both regions evolve towards a common pattern. In the long time limit, a single spiral in each of the regions was all that remained. They also found in simulations that weakly coupled single spirals causes them to move along either cycloidal or straight trajectories when both spirals share the same orientation or have opposite orientations, respectively.

In Ref. [28], we reported the results of experiments and simulations similar to those of Hildebrand *et al.* [27]. We observed synchronized epicycloidal trajectories for spirals with the same chirality and straight trajectories for spirals with opposite chirality. We also found that the spiral cores are attracted to orbits in which the separation between the two cores in different domains are quantized with integer values of half the spiral wavelength. We further developed an analytical model to explain these observations in terms of "kicks" to the core, small location and phase changes of the core following an encounter with a wave front in the other domain.

Here we report on the effects of coupling two separate, two-dimensional domains of the BZ reaction. We previously showed the existence of quantized orbits in simulations [28]; here we show that the same quantization is present in experiments. In addition, we report on the role of coupling strength and initial conditions. The paper is structured as follows. Section II presents our numerical and experimental methods. Section III A explains and discusses the difference between the weakly and strongly coupled regimes. Section III B focuses on experimental and numerical results for weakly coupled systems and the dependence on initial conditions.

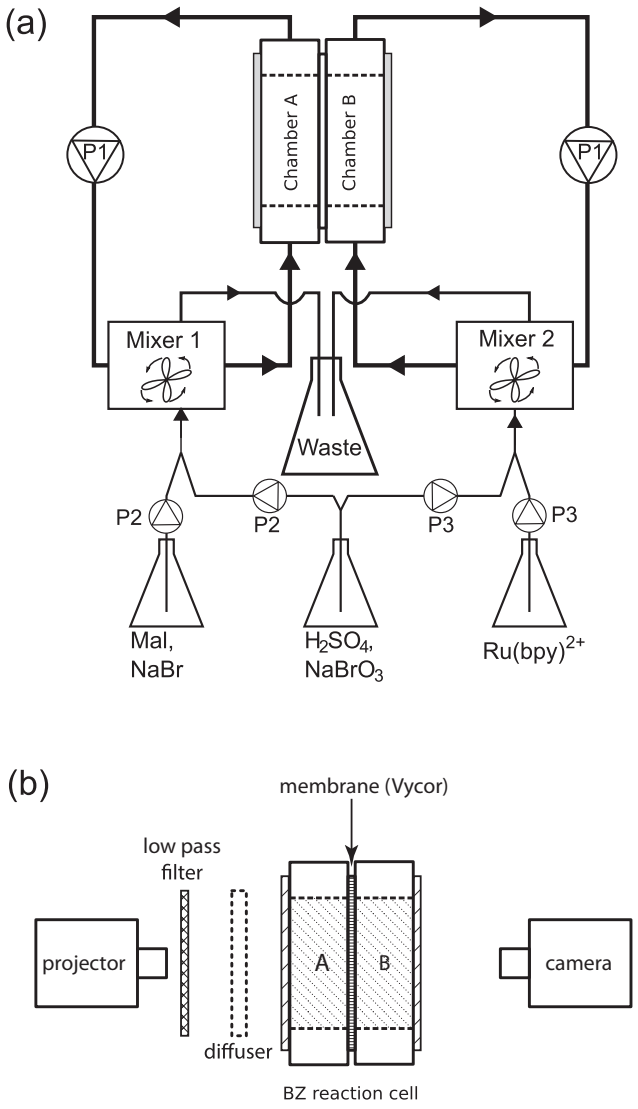

FIG. 2. Schematic of the experimental setup. (a) Reactor and the pump arrangement. Arrows mark directions in which the chemical solutions are pumped. (b) Optical arrangement (see text for explanation).

Sections III C and III D focus on the strongly coupled regime and the transition from weak to strong coupling.

II. METHODS

A. Experiment

Our experiments were preformed with a continuously fed unstirred tank reactor, similarly to the one reported by Ouyang and Swinney [29] and later used by many others [5,17,30]. The schematic is shown in Fig. 2(a). The reactor consists of two chambers separated by a porous membrane (a Vycor glass disk) through which the species diffuse from chamber A and B, meet, and react. The disk had a thickness of 0.5 mm and an open diameter of 2 cm. Chamber A was filled with an aqueous solution of sodium bromide (NaBr) at a concentration of 0.02 mol/l, malonic acid (Mal) at 0.1 mol/l, sulfuric acid (H_2SO_4) at 0.5 mol/l, and sodium bromate ($NaBrO_3$) at

0.15 mol/l. Chamber B was fed by a solution containing the light-sensitive catalyst (2,2′-bipyridyl)dichlororuthenium $[Ru(bpy)_3{}^{2+}]$ at a concentration of 0.5×10^{-3} mol/l, H_2SO_4 at 0.5 mol/l, and $NaBrO_3$ at 0.15 mol/l. As shown in Fig. 2(a), the chemical solution in both chambers was recirculated by a peristaltic pumps (P1) at a high flow rate (170 ml/h) such that the contents of the chambers (volume 4.5 ml) was renewed every 95 s. Depletions of the reactants was counterbalanced by the addition of fresh solution to mixers inline with the recirculation loop at a rate of 20 ml/h for chamber A and 5 ml/h for chamber B. Excess fluid in the recirculation loop was routed to a waste bottle.

Figure 2(b) shows the optical arrangement of our experiment consisting of a computer controlled video projector (Optoma TX542), a shortpass filter (475-nm cutoff wavelength, Edmund Optics), a diffuser (opal diffusing glass, Edmund Optics) mounted on a flipper so it could be removed from the optical path, the reactor, and an 8-bit monochrome camera (PixeLink-E531MU) equipped with a 12- to 36-mm f2.8 zoom lens (Computar). The projector was used both for illumination during image acquisition and for forcing. During image acquisition the diffuser was inserted into the optical path to provide a uniform background, and the projector was set to project a black image at which setting the minute light leakage from the DLP-micro-mirror array provided sufficient illumination for imaging purposes. The shortpass filter rendered areas in the red, reduced state $[Ru(bpy)_3{}^{2+}]$ as dark, and the green, oxidized state $[Ru(bpy)_3{}^{3+}]$ as light. During forcing the diffuser was removed from the optical path and an image was projected onto the membrane.

The image acquisition-forcing cycle consisted of inserting the diffuser, projecting a uniformly "black" image, acquiring an image, processing the image (described below), removing the diffuser, and projecting the processed image. This sequence lasted approximately 2 s, a period short in comparison to the typical spiral period of more than 50 s. (The homogeneous oscillation period is even longer.) The forcing phase occupied approximately 50% of this cycle.

The membrane was subdivided into two separate circular reaction domains 8.6 mm in diameter. This separation was achieved by illuminating the remainder of the disk (i.e., the areas outside the two domains) with an intensity sufficient to stop the reaction and thus waves were unable to cross from one domain to the other.

The gray-scale image from the camera was converted into a black-and-white image ready for the projector by the following sequence. First, the camera image was divided by a background image in order to remove spatial inhomogeneities in the brightness of the image. The background image was calculated as the average of 230 images acquired prior to starting the experiment. Next, the images was binarized using a dynamic threshold chosen such that 40% of pixels lay above the threshold. A dynamic threshold was necessary to compensate for small difference in the average gray value of an image caused by fluctuations of the projector output and differences in the lowest and highest gray values in the forced and the unforced system from which the background was taken. While this forcing scheme differs from the one used in our simulations for which the threshold was constant at all times, the difference is slight and the outcome is qualitatively identical. We note that the observations presented here are qualitatively robust irrespective of the exact choice of the threshold. A change of the threshold, however, would change the observations quantitatively. For example, the spiral rotation rate, the spiral wave number, or the spiral decay rate as discussed in Sec. III B 2, would slightly differ for different thresholds. Finally, the image was flipped so when projected onto the reactor the binarized image of domain 1 overlaid domain 2 and vice versa. Failure to have proper registration between the image and its projection leads to a nonlocal interaction and in experiments produces drift (see below). Thus, great care was taken to ensure that if the image of a point in domain one x_1 was projected onto domain two at x_2, then so, too, was the image of x_2 projected onto x_1.

In the following, we use the relative intensity $\mathcal{I}$ as a measure of the coupling strength, with $\mathcal{I}$ normalized to unity at the maximum intensity achievable with our projector ($250\,W/m^2$). Note that the physical value of the light intensity by itself is insufficient for comparison with other experiments, since light sensitivity of the reaction depends strongly on the chemical concentrations of all species.

B. Numerical simulation

The two-variable Oregonator model [31,32] with forcing (see, for instance, Refs. [23,33]):

$$\partial_t u_i = \nabla^2 u_i + \frac{1}{\epsilon}\left[u_i - u_i^2 - (f v_i + I_i)\frac{u_i - q}{u_i + q}\right]$$
$$\partial_t v_i = D_v \nabla^2 v_i + u_i - v_i \qquad (1)$$

was integrated using an Euler scheme. Here u represents the concentration of the autocatalytic reactant (hydrobromous acid, $HBrO_2$), v is the concentration of the oxidized catalyst $[Ru(bpy)_3{}^{3+}]$, and I is the additional bromide production induced by illumination of the system. The constants ϵ, q, and f depend on the concentration of the other species and the specific reaction kinetics. The domain number $i = [1,2]$.

In our experiments both species u and v diffuse. In the absence of data on the diffusivity of the catalyst, we assume it scales as the cube root of its molecular mass. This yields a diffusivity half that of u. However, we note that the exact value is rather unimportant and that our simulations are comparable with simulations assuming a nondiffusive catalyst. In fact, for $D_v = 0.5$ the spiral rotation rate is equal (within 0.5%) to the spiral rotation rate for $D_v = 0$.

The parameter values were fixed at values given in Table I. For these parameters, the homogeneous system is in the oscillating regime, i.e., the entire domain oscillates

TABLE I. System parameters. Experiments: Chemical concentrations in chamber A and B. Simulations: Parameters for Eq. (1).

Experiments	A	B	Simulations	
Sodium bromide	0.02 M	–	f	1.5
Malonic acid	0.1 M	–	q	0.0015
Sulfuric acid	0.5 M	0.5 M	ϵ	0.08
Sodium bromate	0.15 M	0.15 M	D_v	0.5
Ruthenium complex	–	0.5 mM	I_0	0–1

uniformly in the absence of spirals. Nevertheless, since the spiral frequency is faster than the frequency of homogeneous oscillations, spirals once nucleated will dominate. For these parameters and $I_i = 0$ (uncoupled), spiral cores are stationary and spiral patterns undergo steady rotation with period of 3.56.

The forcing term $I_i(\mathbf{x},t)$, was calculated as follows:

$$I_i(\mathbf{x},t) = \begin{cases} I_0 & : v_j(\mathbf{x},t) \geqslant v_t \\ 0 & : v_j(\mathbf{x},) < v_t \end{cases} \quad \text{with} \quad i \neq j.$$

Here I_0 is the coupling strength, and v_t is a threshold value that is calculated as

$$v_t = (v_{\min} + v_{\max})/2,$$

where $v_{\min}$ and $v_{\max}$ are the minimal and maximal values of v occurring during a single cycle in the unforced homogeneous Oregonator model with these parameters. Two dimensional simulations where conducted on a 580×580 grid and advanced in time using an Euler scheme with time steps $\Delta t = 0.001$ and the grid spacing $\Delta x = 0.2$. In the figures below showing simulations results, the v field is plotted because then light areas in both experiments and simulations correspond to high $Ru(bpy)_3^{3+}$ concentrations.

III. RESULTS

A. Weak versus strong coupling

The results of coupling two BZ reactions depend on the coupling strength (I_0 for simulations or $\mathcal{I}$ for experiments) and the chemistry [concentration of the reactants for experiments or parameters f, ϵ, and q in Eq. (1) for simulations]. Here we focus on the role of the coupling strength by fixing the chemistry. We find that as the coupling strength increases there is a qualitative change in the synchronization of the system; below we refer to the phases on either side of this transtion as the *weakly coupled* and *strongly coupled* regimes.

The weakly coupled regime is characterized by an interdomain interaction between wave fronts that slows the propagation of both wave fronts but does not break them. This effect is illustrated in Fig. 3(a): Wave fronts that without coupling are uniformly curved (see Fig. 1) develop kinks where their advance has been retarded by an interaction with a wave front in the other domain. Crucially, at no point is the effect sufficient to break the wave front.

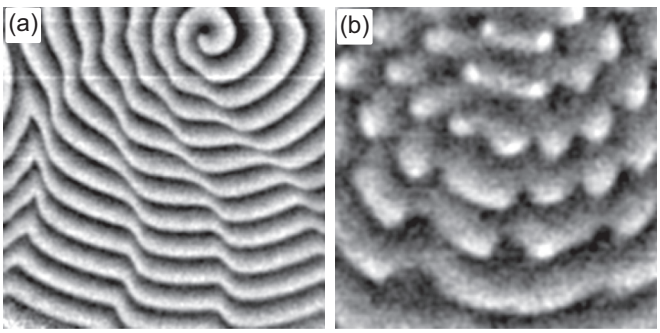

FIG. 3. (a) At weak forcing, wave fronts are distorted due to a local decrease of their propagation speed. The coupling strength here was $\mathcal{I} = 0.4$. (b) At strong forcing, wave fronts break and give rise to new spiral cores. The coupling strength here was $\mathcal{I} = 0.7$.

Coupling of any magnitude causes cores to become mobile. In the weakly coupled regime no new spirals can form but spirals are destroyed by collisions with the boundary or with an oppositely handed spiral. Therefore, the number of spirals can only decrease or remain steady in time. This effect is discussed more fully below in Sec. III B 2.

In the strongly coupled regime the interdomain interaction is sufficiently strong to suppress the reaction and thus wave fronts break wherever the intensity exceeds a certain threshold. The two newly created ends curl up to form two new counter-rotating spiral cores. This situation is illustrated in Fig. 3(b) that shows the resulting wave fronts almost immediately after the coupling was turned on. Thus, the number of spiral cores can increase with time provided it outpaces the annihilation mechanisms mentioned above (see also, e.g., Fig. 9). In our experiments, the transition from weak to strong coupling occurs at $\mathcal{I} = 0.45$. We reiterate that the exact value depends highly on the chemical concentrations. For example, the strongly coupled regime is beyond the maximum intensity of our projector when the concentration of $NaBrO_3$ is increased to 0.3 mol/l. Between the weakly and strongly coupled regimes there is a small transition regime wherein wave fronts can break but do not always do so depending on the history at the specific location (see also Sec. III D).

B. Weak coupling

1. *Experimental coupling of two corotating spirals*

Without coupling, spiral waves are stationary for our experimental conditions and simulation parameters: The tip of the spiral circles a stationary core. With coupling, cores become mobile because the tip of the spiral is perturbed every time it meets—virtually—a wave front in the other domain. Henceforth, we refer to the motion of the cores in both domains as though they occur on a single virtual plane defined by superimposing both domains so points that are coupled lie on top of each other. In Ref. [28] we showed in experiments and simulations that if each domain is occupied by a single spiral wave, then the coupling between the domains causes an effective attraction between their cores. We further showed in simulations that when both waves have the same handedness the cores orbit a common center with diameters that are integer multiples of half the spiral wavelength and at any instant they lie on diametrically opposing sides of the center.

We define the spiral wavelength as the average distance between consecutive wave fronts. The wavelength without forcing λ_0 is spatially uniform and is 0.66 ± 0.03 mm in experiments. With forcing the motion of the core causes a Doppler-like distortion of the spacing between wave fronts depending on the direction of motion at the instant the wave front is emitted; the spatially averaged wavelength in experiments with forcing λ is 0.69 ± 0.03 mm, about 5% larger than λ_0.

In Ref. [28] we developed an analytical model for the core trajectories based on a single ingredient: A wave front striking a tip imparts a deterministic translation and phase delay ϕ of the tip. The model predicts orbits spaced at radii

$$R(m) = \left(m + \frac{1}{2} - \frac{\varphi}{\pi}\right)\frac{\lambda}{4}. \tag{2}$$

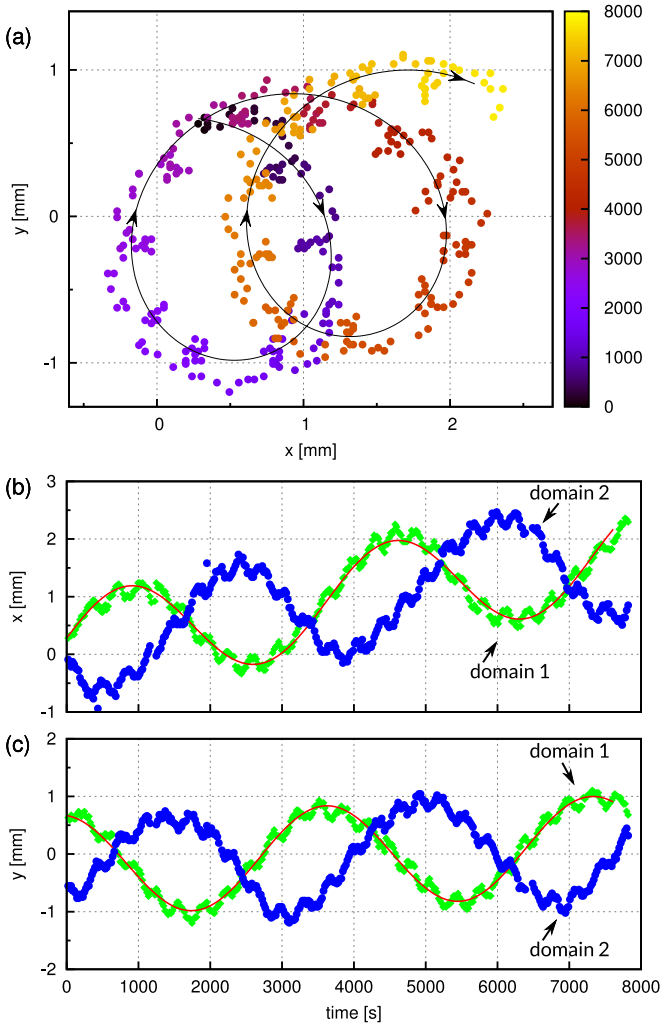

FIG. 4. Typical example of a spiral tip trajectory in experiments in the weakly coupled regime. Solid circles in (a) mark the positions of the spiral in the xy plane of domain one for different times (indicated by the symbol color - see color bar). Panels (b) and (c) show separately the x and y coordinates versus time for the spirals in both domains. Solid lines in (a), (b), and (c) are fits of Eq. (3) for the position of the spiral tip in the first domain.

The stability of the orbit with radius $R(m)$ depends on the relative phases of the cores. Defining $\Delta\psi \equiv \psi_1 - \psi_2$ as the difference in phases of spirals (see Fig. 1) in domain 1 and 2, orbits with radii $R(m)$ are stable for even m and $\cos(\Delta\psi) > 0$ or for odd m and $\cos(\Delta\psi) < 0$. In simulations $\Delta\psi \to 0$ or π at long times, depending on the initial conditions; in our analytically model ψ is an input parameter.

Here we report for the first time experimental evidence of this quantization. We conducted experiments with various initial core-core separation of two spiral waves with the same handedness. We find, in contrast to simulations, that the cores exhibit circular trajectories with a superimposed drift (see Fig. 4). We attribute the drift to imperfect alignment of the optical path in the experiment and inhomogeneities of the membrane that cause small variations of the spiral frequencies across the reactor.

We subtract this drift by fitting the core position $\mathbf{r}_i = \binom{x_i}{y_i}$ in domain i to

$$\mathbf{r}_i(t) = \mathbf{r}_{0i} + \mathbf{v}_i t + R_i \begin{bmatrix} \cos(\Omega_i t + \Theta_i) \\ \sin(\Omega_i t + \Theta_i) \end{bmatrix}, \tag{3}$$

where R_i is the orbital radius, Ω_i the rotation frequency, Θ_i the phase of a circular core trajectory for domain $i = \{1,2\}$, and $\mathbf{v}_i$ is the drift. An example of the experimentally measured core trajectory with a typical drift is shown in Fig. 4(a) on the x-y plane and in Figs. 4(b) and 4(c) for each component as a function of time. The trajectory of each tip is well approximated by an epicycloid, i.e., the curve generated by a point on a disk rolled around the circumference of a smaller circle. Thus, the trajectories in Figs. 4(b) and 4(c) show a fast small-amplitude oscillation superimposed on a slower large oscillation (and a constant drift $\mathbf{v}$). The small oscillations correspond to the rotation of the tip around the core. Since the core motion is our primary interest, we did not attempt to resolve the small oscillation and neglected the corresponding terms in our fit [Eq. (3)]. With this caveat in mind, Eq. (3) fits the data well.

Figures 4(b) and 4(c) show the x and y positions of the spiral tips in their respective domains. We note that both spirals drift roughly in the same direction with very similar velocities $\mathbf{v}_1$ and $\mathbf{v}_2$. That the drift is along a linear path suggests that misalignment of the optics is the primary cause of the drift because if it were due to frequency differences of the spirals the drift would be along a curved path. Once the drift is subtracted, the cores follow circular orbits around a common center point on diametrically opposite sides with quantized radii. This behavior is in accord with the simulations. However, unlike in simulations, the radii of these circular orbits [R_i in Eq. (3)] are not necessarily equal.

Figure 5 (inset) shows a plot of R_1 versus R_2 measured from fitting Eq. (3) to the data from 19 experimental runs. The clustering of data points around particular values and the gaps between neighboring clusters are manifestations of the quantization of the radii. The best fit to Eq. (2) yields a value for $\lambda = 0.7$ mm which is equal within experimental uncertainty to the spiral wavelength with forcing λ. Figure 5 shows the inset data replotted with the radii normalizing by λ. The degree to which the system exhibits quantization is attested by the proximity of the data to integer values of $R/(\frac{1}{4}\lambda)$. The most common case is that both radii are the same (i.e., $m_1 = m_2$) but there are a few instances where $m_2 = m_1 + 1$. For small orbits ($m \leqslant 4$) the quantization is clear and for larger orbits less so.

While Fig. 5 confirms the existence of quantization in the experimental system predicted by simulations, the experiments differ from the simulations in that (1) R_1 and R_2 are not necessarily equal and (2) the quantization appears to weaken for large separations. We argue that both issues are due to idealizations implicit in the simulations.

The first idealization in simulations is constancy of spiral frequencies across domains. However, experiments show that the spiral frequency in domain 2 is systematically higher than in 1 by as much as 4% even though both domains nominally share the same substrate and are exposed to the same chemical gradients. (These differences are likely due to

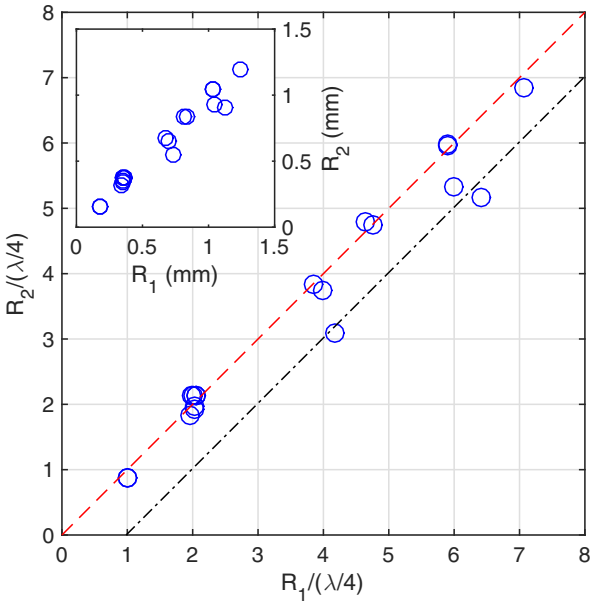

FIG. 5. Radii of orbits in domain 1 and 2 plotted against each other. Radii are normalized by a fitted value of the wavelength over four to highlight the m dependence in Eq. (2); the fit yields a value of $\lambda = 0.70$ mm and $\varphi = 1.5$ rad. The clustering of data around integer values of $R_i/(\frac{1}{4}\lambda)$ is indicative of quantization. While most orbits have equal radii [i.e., $R_1(m) = R_2(m)$; red dashed line], we observe some instances of orbits with $R_1(m) = R_2(m+1)$ (dash-dotted line). Inset: Un-normalized radii.

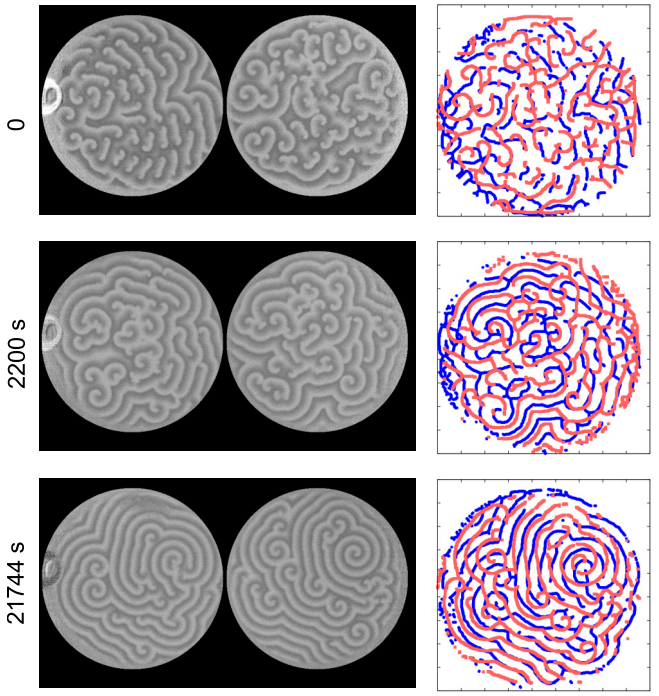

FIG. 6. Evolution of initially random BZ patterns for an experiment in the weakly coupled regime ($\mathcal{I} = 0.15$). Left: Gray-scale image of both domains. Right: Skeletonized image showing superimposed wave fronts extracted from the left [dark (blue)] and right [light (red)] domains. The small circular mark on the left side of the left domain is a small air bubble attached to the window of the reaction chamber; it did not affect the reaction pattern.

inhomogeneities in the substrate that result in variations of the diffusion coefficient across the membrane.) If spiral 2 is rotating faster, then core 1 will receive more kicks per unit time than core 2, and thus, according to our model, core 1 will travel a greater distance. Since $R_1 \geqslant R_2$ as seen in Fig. 5, it is plausible to attribute the cases where $R_1 \neq R_2$ as the result of differences in the rotational rates.

The second idealization in simulations is perfect registration between domains. In experiments the presence of drift attests to some degree of misalignment in the experimental system. Furthermore, the effect of drift is greater for larger orbits because the long duration and large trajectory of the orbit exacerbates experimental issues due to variations in the membrane diffusivity, optical distortions, fitting accuracy, and so on. We ascribe the imperfect quantization for large orbits to these issues.

2. *Random initial conditions*

Here we describe the results of weak coupling for initial conditions consisting of multiple randomly positioned spiral cores. Figures 6 and 7 show examples of the evolution with time of such patterns in experiments and simulations.

We prepared the initial state of these experiments by first allowing the system to develop naturally. This typically produced several randomly positioned spiral cores. Once this state reached steady state, we projected a short-duration high-intensity, artificially generated, spiral pattern that chopped the wave fronts into small pieces from which new cores were formed. We then coupled the resulting patterns and followed their evolution in time.

Figure 6 shows a typical example of the evolution of the system from random initial conditions. Initially (at $t = 0$), the wave fronts are short and there is no obvious alignment of fronts between domains. Later (at $t = 2200$ s ≈ 42 rotational periods) the number of spiral cores has decreased, the extent of any given spiral wave has increased, and there are patches of interdomain wave-front alignment (e.g., at the bottom). The latter is particularly evident in the skeletonized image. Much later ($t = 21744$ s ≈ 430 rotational periods), there is a strong alignment of the wave fronts.

This progression is reproduced in simulations as shown in Fig. 7 and is even clearer because we are able to observe the evolution over more initial configurations and for longer time spans. At $t = 114$ (corresponding to 28 spiral rotation periods) in Fig. 7 the number of cores is highly reduced from its value at $t = 0$ and the degree of alignment between domains is easily discernible. By $t = 424$ (102 rotation periods), the cores of the largest spiral waves are on top of each other. The phase of paired-up spirals differ by about 180°, such that wave fronts of one domain are in between wave fronts of the other in their superimposed coordinate system. In summary, the most notable behaviors of weakly coupled domains with a random distribution of cores are that with time the number of cores decreases, cores pair up with a partner in the other domain, and once the cores are coincident wave fronts are aligned.

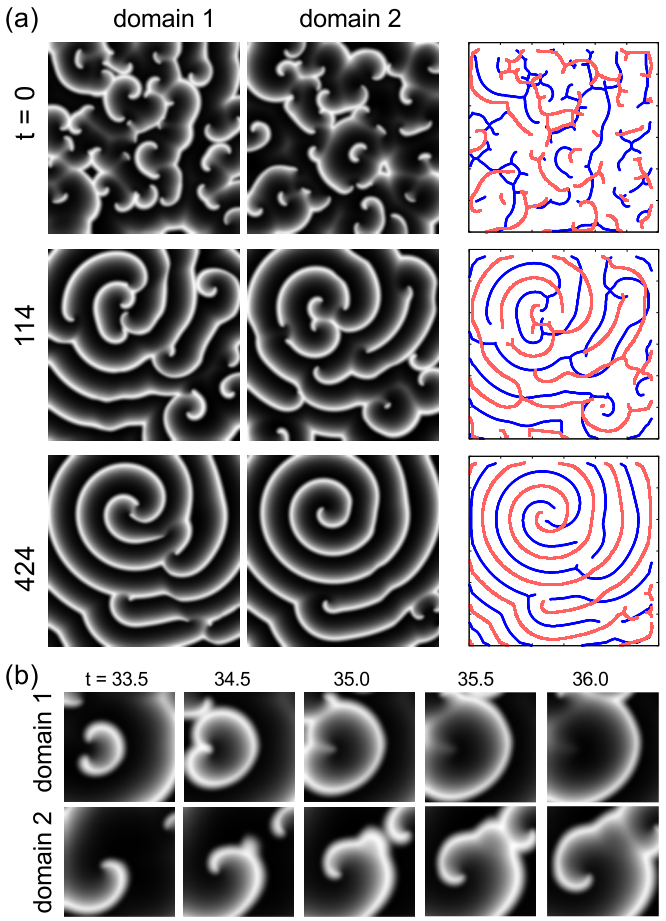

FIG. 7. (a) Evolution of weakly coupled initially random BZ patterns in the simulation. Gray images of both domains are shown at the left side. The right column shows the extracted wave fronts of the first [dark (blue)] and the second domain [bright (red)] superimposed on each other. (b) Spiral core annihilation. Two counter-rotating spiral cores merge and subsequently disappear. In this way, spiral cores are destroyed, leading to an increasing synchronization of the patterns.

Our experiments with single cores suggest the following mechanism for this progression towards synchronization. The interdomain interaction causes the core in one domain to move as it is buffeted by wave fronts in the other domain. This motion is erratic—akin to a random walk—in the long term because over its lifetime the core interacts with multiple cores in the other domain. If, however, a core encounters the edge of the domain or a core with the opposite chirality (in its own domain), it is annihilated. Since there is no core creation mechanism, the number of cores decreases monotonically with time. The erratic motion of the core will only cease when it pairs up with a core with the same chirality in the opposite domain. Thus, paired cores will survive provided their orbit does not intersect the boundary. Survival is most likely when the cores lie on top of each other because the orbit is very small. Thus, in the long term a few bound cores remain.

To examine this scenario we measured the number of cores versus time from simulations (see Fig. 8). The counts were obtained by skeletonizing the gray image and counting the end points of each wave front. This method is fast but

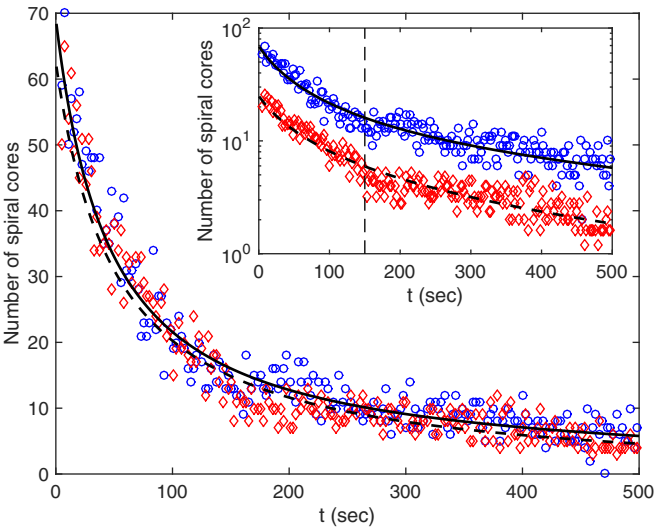

FIG. 8. Number of spiral cores as a function of time for the simulation shown in Fig. 7 for domain 1 (○) and domain 2 (◇). The dashed and dotted lines mark fitted solutions $n_1(t)$ and $n_2(t)$ of Eq. 4. Inset: Same data plotted logarithmically; data for domain 2 (◇) shifted downwards for clarity. The vertical dashed line at $t = 155$ marks a transition suggested by the change of the slope.

undercounts the true value because the end of the wave front may touch another wave front during a brief interval of the period so it is not visible in the skeletonized image. Thus, our count can fluctuate upward or increase on short time scales, even though no new spiral cores form. Discounting these fluctuations because they are artifacts, the number of spiral cores decreases monotonically in time with equal rates in both domains. These data show that (i) the number of cores in each domain are roughly equal at all times and (ii) the decay is exponential with a time constant that changes abruptly at $t \approx 150$ s from faster to slower (see Fig. 8, inset).

We attempted to model the observed decrease in spiral cores using the annihilation mechanisms described above. Our model describes the dynamics in terms of four variables $n^{(i)}_{\{r,l\}}$, the number of right- or left-handed spirals in the ith domain. Their evolution is given by the following system of equations

$$\dot{n}^{(i)}_r = -\alpha n^{(i)}_r - \beta n^{(i)}_r n^{(i)}_l$$
$$\dot{n}^{(i)}_l = -\alpha n^{(i)}_l - \beta n^{(i)}_r n^{(i)}_l, \qquad (4)$$

where the first term on the right-hand side accounts for cores leaving the domain and the second term accounts for annihilation of oppositely handed cores.

At early times there are many cores and so the second term is dominant; at later times when few cores remain, these are more likely to encounter the boundary than each other, and so their number decreases exponential with a $1/e$ time constant of α^{-1}, consistent with the observed exponential at late times [see Fig. 8 (inset)]. Moreover, we observed in simulations that for larger domains the spiral number decrease due to the lateral boundaries becomes less important and that the onset time for the long-time exponential decay increases.

Since our data do not distinguish between left- and right-handed cores, we compare the total number of cores

$n_i = n_r^{(i)} + n_l^{(i)}$ given by Eq. (4) with our data in Fig. 8. A least-squares fit to the model yields $\alpha = 1.0 \times 10^{-3}$ s and $\beta = 3.5 \times 10^{-4}$ s. The model captures well the overall trend and the late time exponential but does not display the early time exponential presumably because of the overly simple interaction term $n_l n_r$ in Eq. (4).

C. Strong coupling

An example of the evolution of a strongly coupled system in experiments is shown in Fig. 9. The initial patterns ($t = 0$) consist of multiple spirals irregularly distributed about the domains. The skeletonized wave fronts (right column) show no particular alignment between domains or correlations of core locations.

With time the coupling causes the wave fronts to weaken, and eventually break, wherever they intersect a wave front in the other domain. New spiral wave subsequently develop from the free ends where the wave fronts broke. The magnified view in Fig. 10 illustrates the details of this process. Due to the creation of new spirals and the inhibition of propagation of wave fronts that do not coincide with a wave front in the other domain, the pattern of wave fronts synchronize so the wave fronts in both domains are aligned and in phase with each other. Synchronization is achieved rapidly; in the example shown in Fig. 9 the two domains are almost completely synchronized by 151 s, approximately three rotational periods.

In simulations we observe the same processes driving the system towards a synchronized state but with one major difference: Wave fronts are shifted by π across domains. So instead of identical patterns in both domains as in experiments, the resulting patterns are complements of each other (see Fig. 11).

Clearly, the photosensitive Oregonator model does not accurately capture the experimental system. The problem originates in the form of the coupling. The photosensivity in the Oregonator was proposed as the "simplest necessary modification" of the original Oregonator to include the effects of illumination [33]. The modification consisted of augmenting the production of the inhibitor Br^- in proportion to the intensity of light, i.e., $fv \to fv + I$ in Eq. (1). However, subsequent studies by Kádár *et al.* established that the production of Br^- is mediated by $Ru(bpy)_3^{2+}$ and thus its presence is necessary for inhibition. Therefore, illuminating bright areas, which are high in $Ru(bpy)_3^{3+}$ and low in $Ru(bpy)_3^{2+}$, forces the system much weaker than illuminating dark areas [high in $Ru(bpy)_3^{2+}$ and low in $Ru(bpy)_3^{3+}$].

The patterns observed in experiments are consistent with this $Ru(bpy)_3^{2+}$ dependence, and the waves from opposite domains line up peak to trough so they inhibit each other minimally. When the patterns in both domains are the same, either high-intensity light is projected onto regions of high $Ru(bpy)_3^{3+}$ concentration and thus low $Ru(bpy)_3^{2+}$ concentration, or low-intensity light is projected onto regions of high $Ru(bpy)_3^{2+}$ concentration. In either case, the local inhibition of the reaction is weak. Conversely, high-intensity light on dark regions is highly inhibitory.

Contrary to experiments, the effective coupling in the Oregonator model [Eq. (1)] between domains is least when the patterns do not overlap. Regions with high v_1 produce high

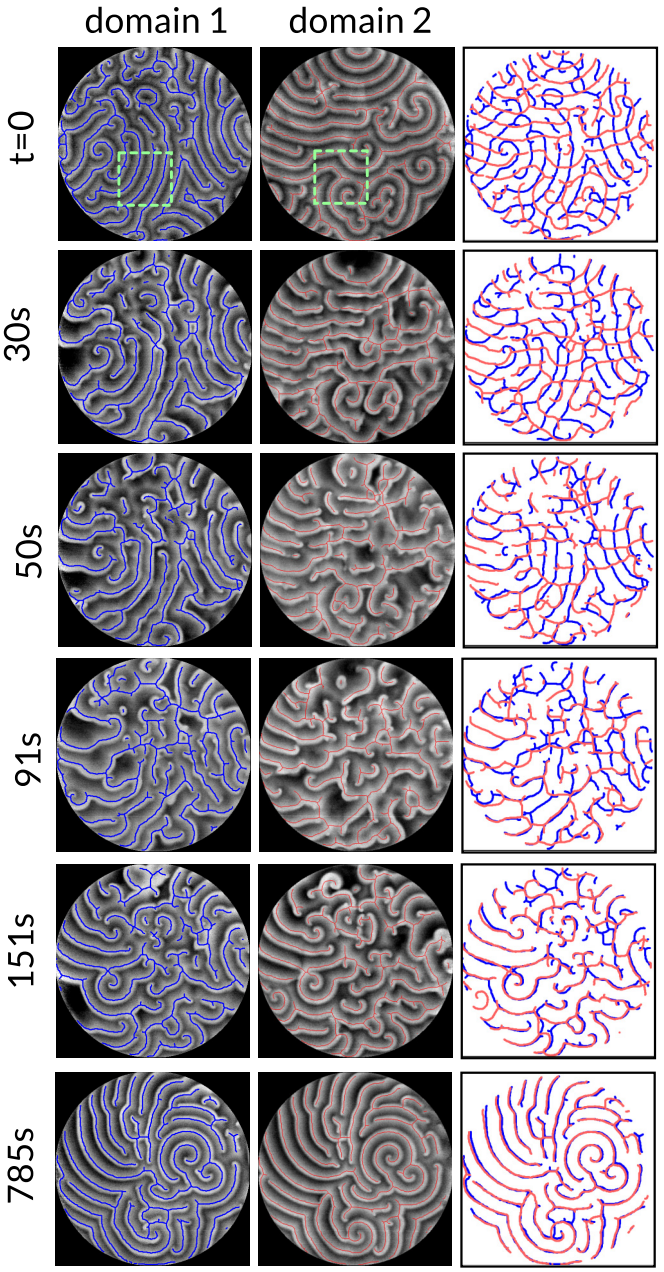

FIG. 9. Time evolution of strongly coupled spiral patterns in the experiment ($\mathcal{I} = 0.5$). The left and middle columns show the extracted wave fronts superimposed on the gray-scale pattern for various times. The right column shows the superposition of the wave fronts from cell 1 [dark (blue)] and cell 2 [bright (red)]. The region within the dashed square (green) is used in Fig. 10. The rotation period of the undisturbed spirals was 48 s.

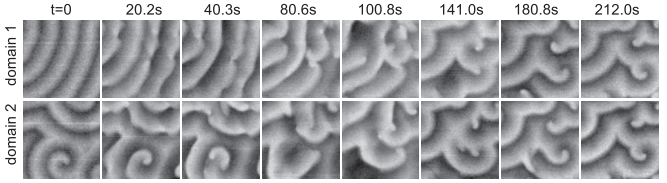

FIG. 10. Fragmentation of wave fronts and formation of new spirals during the evolution towards synchronization. Images cropped from Fig. 9.

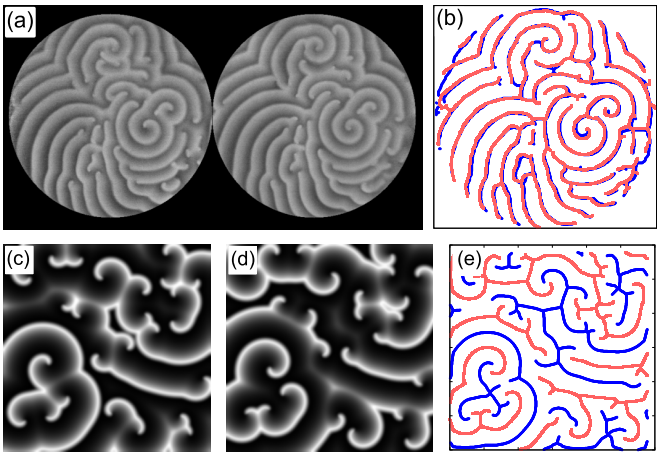

FIG. 11. Wavefront patterns synchronized by strong coupling in (a) experiments and [(c) and (d)] simulation. Bright areas correspond to high concentration of the oxidized catalyst $[Ru(bpy)_3]^{3+}$ in the experiment, v in the simulation]. [(b) and (e)] Wavefronts extracted from (a), (c), and (d) illustrating the degree of synchronization.

forcing in domain 2 which in turn is inhibitory only in regions with large u_2 and vice versa. However, if the patterns are intercollated as in Fig. 11(e), the effective coupling is weakest because high forcing falls on regions of low v (and low u since v follows u closely).

Though there are models [19,34] that incorporate more sophisticated treatments of the chemical kinetics that may resolve this discrepancy, we did not implement these.

D. Characterizing the transition from weak to strong coupling

We investigated the degree of synchronization with the aim of identifying an order parameter to distinguish weak from strong coupling. These simulations were performed using a random spiral configuration as the starting condition. To analyze the pattern in time, we first calculated phase fields $\phi_i(x,y,t)$ at each point in space (x,y) by mapping the time interval between two consecutive maxima in v_i onto the phase interval 0 to 2π.

Figure 12 shows examples of $\phi_i(x,t)$ and the phase difference between domains 1 and 2,

$$\Delta\phi(x,t) = (\phi_1(x,t) - \phi_2(x,t)) \mod 2\pi$$

for weak [Figs. 12(a)–12(c)] and strong forcing [Figs. 12(d)–12(f)]. For weak forcing [Fig. 12(c)], the phase difference varies across the domain and assumes all values between 0 and 2π, whereas for strong forcing [Fig. 12(f)] the phase difference is everywhere close to π except in the vicinity of spiral cores where our method yields a phase singularity.

We then calculated the time-dependent root-mean-square difference $\sigma_s(t) = \sqrt{\langle(\Delta\phi - \langle\Delta\phi\rangle_s)^2\rangle_s}$, where $\langle\rangle_s$ denotes the spatial average at fixed time. Figure 13 is a plot $\sigma_s(t)$ for different coupling strengths (denoted by line color). For zero and very weak coupling, $\sigma_s \approx 1.8$. Since $\pi/\sqrt{3} \approx 1.81$ is the value expected for uncorrelated phase fields, we conclude that for $I_0 \lesssim 0.03$ there is no synchronization. For large coupling strength ($I_0 \gtrsim 0.1$) σ_s decreases sharply at the beginning

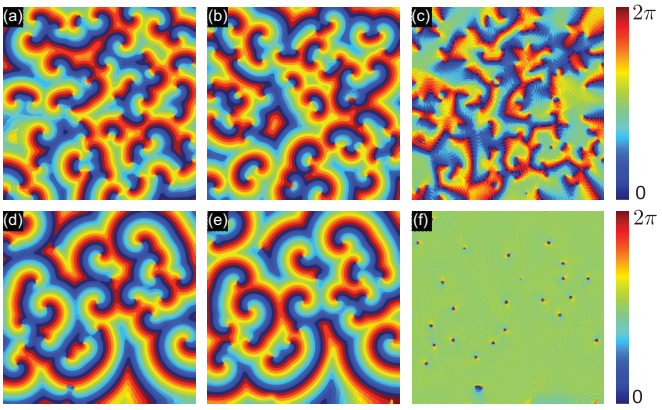

FIG. 12. Phase of domains 1 [(a) and (d)] and 2 [(b) and (e)], and their pointwise difference [(c) and (f)] for weak ($I_0 = 0.03$, top row) and strong coupling ($I_0 = 0.16$, bottom row).

and reaches a plateau with $\sigma_s \approx 0.3$, a value we take to be, based on visual inspections of the fields, equivalent to full synchronization. Note that even though theoretically full synchronization ought to have $\sigma_s = 0$ (i.e., $\Delta\phi(x) = \langle\Delta\phi\rangle_s$ for all x), in practice the presence of phase singularities in our computations raises this value to approximately 0.3.

At intermediate values of the coupling strength σ_s initially decreases slightly and then fluctuates strongly. The initial decrease is due to attrition of spiral cores by the mechanisms discussed in Sec. III B 2. The spirals that survive this initial phase pair up with partners in the other domain and orbit each other. Due to the finite size of our system and the small number of cores present, the phase differences vary greatly in time because of variations of pattern from the orbital motion of the core and occasional collisions of a core with the domain boundary.

These qualitative observations are quantified in Fig. 14, which shows $\langle\sigma_s\rangle_t$, the time-averaged σ_s minus $\pi/\sqrt{3}$, and the standard deviation in time of σ_s, $\sqrt{\langle(\sigma_s(t) - \langle\sigma_s\rangle_t)^2\rangle_t}$, plotted versus I_0. The time averages were computed for $t > 40$ (denoted by the black vertical line in Fig. 13) in order to eliminate transients. These data show the hallmarks of

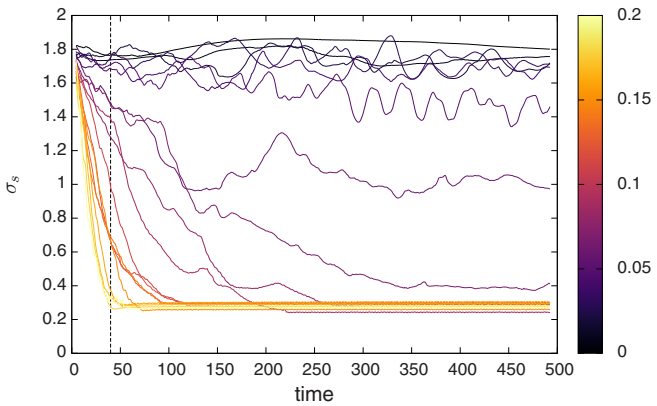

FIG. 13. Spatial standard deviation of the phase differences between domain 1 and domain 2, as a function of time for different coupling strength I_0 (color coded). The dashed vertical line marks an arbitrary chosen threshold $t_t = 40$. Only data for $t > t_t$ were used to calculate statistical properties shown in Fig. 14.

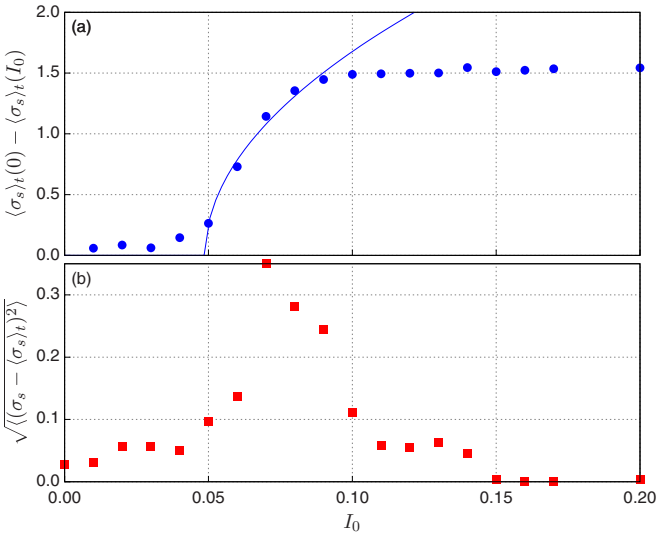

FIG. 14. (a) The difference between the average σ_s at $I_0 = 0$ and at I_0 (blue circles). (b): The standard deviation (red squares, right y axis) as a function of the coupling strength. These values were calculated based on the times larger than $t_t = 40$ (black vertical line in Fig. 13). The solid line (blue) is a fit of $\propto\sqrt{I_0}$ to the data as expected for a pitchfork bifurcation.

a bifurcation (see, e.g., Ref. [35]): the sudden appearance of an order parameter $\langle\sigma_s\rangle_t$ and strong fluctuations of the order parameter near the transition. Assuming a pitchfork bifurcation, a fit of a square-root function to the data near the onset of strong coupling gives a value of $I_0 = 0.05$ for the transition from weak to strong coupling.

IV. SUMMARY

We investigated experimentally and numerically the effects of point-to-point coupling of two spatially extended light-sensitive Belousov-Zhabotinsky systems in the parameter regime where spiral cores are stationary. Coupling causes the domains to synchronize with modalities that depend on the forcing strength and the initial wave pattern of the BZ reaction.

There are two regimes as function of coupling strength distinguishable by the effect of wave fronts on each other. In the weak-coupling regime wave fronts are locally deformed, due to a reduction of the propagation speed when illuminated, but do not break, whereas in the strong-coupling regime wave fronts break. In both cases, spiral cores are no longer stationary. We showed previously [28] that weak coupling with a single spiral in each of the two domains induces a synchronized state in which the two spirals with the same orientation orbit a common center along circular trajectories. Furthermore, our simulations showed that the radii of these trajectories are quantized with integer multiples of half of the spiral wavelength. Here we showed that the experimental system also exhibits this quantization.

For an initially random spiral pattern in the weak-coupling regime we found that the number of spiral cores decreases in time until the only cores remaining are those that have formed a bound pair with a core in the other domain. Spirals annihilate by collisions with oppositely handed spirals or the boundary, with the former dominating at early times when there are many spirals and the latter dominating at later times when spiral-spiral collisions are rare. The only cores that survive are those whose trajectories are stabilized by forming a bound pair with a core in the other domain.

In the strongly coupled regime patterns synchronize quickly and completely, resulting in nearly identical patterns in both domains regardless of the initial condition. The mechanism for rapid synchronization is wave-front breaking. Wherever two wave fronts from opposite domains overlap, they break and new spiral waves form from the broken ends. The only spiral cores that survive this process are those that share the same position as a core in the opposite domain.

While experiment and simulation agree for weak coupling, they differ for strong coupling. In experiments the pattern become identical in both domains, whereas in simulation they differ by a phase shift of π. This discrepancy indicates a shortcoming of the simplest light-coupled Oregonator model that assumes a production of inhibitor (Br^-) that is proportional to illumination but independent of the concentration of the oxidized catalyst [$Ru(bpy)_3^{3+}$].

Our examination of the crossover from weak to strong coupling revealed a sharp transition. We used σ_s, the standard deviation of the local phase difference between domains 1 and 2, as an order parameter. For weakly coupled domains $\sigma_s \approx \pi/\sqrt{3}$, indicating uncorrelated phase fields, and in the very strongly coupled regime $\sigma_s \approx 0$, indicating complete correlation between domains. The change between these two limits occurs abruptly and is well fit by a pitchfork bifurcation. Furthermore, near the transition the fluctuations in time of $\sigma_s(t)$ peak, consistent with the weakened damping near a phase transition. Thus, we conclude that the transition from weak to strong coupling is a phase transition.

ACKNOWLEDGMENT

We acknowledge support from the James S. McDonnell Foundation (USA).

[1] B. P. Belousov, Sbornik Referatov po Radiatsionnoi Meditsine, 145 (1958).
[2] A. N. Zaikin and A. M. Zhabotinsky, Nature **225**, 535 (1970).
[3] W. Jahnke and A. T. Winfree, J. Chem. Educ. **68**, 320 (1991).
[4] S. K. Scott, *Oscillations, Waves, and Chaos in Chemical Kinetics* (Oxford Science, Oxford, 1994).
[5] A. L. Belmonte, Q. Ouyang, and J.-M. Flesselles, J. Phys. II (France) **7**, 1425 (1997).
[6] A. T. Winfree, Science **181**, 937 (1973).
[7] J. M. Davidenko, A. V. Pertsov, R. Salomonsz, W. Baxter, and J. Jalife, Nature **355**, 349 (1992).
[8] N. Gorelova and J. Bures, J. Neurobiol. **14**, 353 (1983).
[9] G. Seiden and S. Curland, New J. Phys. **17**, 033049 (2015).

[10] J. D. Murray, *Mathematical Biology Vol. II* (Springer-Verlag, Berlin, 1989).
[11] V. Krinsky and K. Agladze, Physica D **8**, 50 (1983).
[12] G. S. Skinner and H. L. Swinney, Physica D **48**, 1 (1991).
[13] A. L. Lin, A. Hagberg, A. Ardelea, M. Bertram, H. L. Swinney, and E. Meron, Phys. Rev. E **62**, 3790 (2000).
[14] A. S. Mikhailov and K. Showalter, Phys. Rep. **425**, 79 (2006).
[15] J. N. Demas and D. Diemente, J. Chem. Educ. **50**, 357 (1973).
[16] V. Petrov, Q. Ouyang, G. Li, and H. L. Swinney, J. Phys. Chem. **100**, 18992 (1996).
[17] K. Martinez, A. L. Lin, R. Kharrazian, X. Sailer, and H. L. Swinney, Physica D **168-169**, 1 (2002).
[18] S. Kiádár, T. Amemiya, and K. Showalter, J. Phys. Chem. A **101**, 8200 (1997).
[19] S. Nakata, M. Matsushita, T. Sato, N. J. Suematsu, H. Kitahata, T. Amemiya, and Y. Mori, J. Phys. Chem. A **115**, 7406 (2011).
[20] O. Steinbock, V. Zykov, and S. C. Müller, Nature **366**, 322 (1993).
[21] V. S. Zykov, O. Steinbock, and S. C. Müller, Chaos **4**, 509 (1994).
[22] R.-M. Mantel and D. Barkley, Phys. Rev. E **54**, 4791 (1996).
[23] S. Zykov, V. Zykov, and V. Davydov, Europhys. Lett. **73**, 335 (2006).
[24] B. Marts, A. Hagberg, E. Meron, and A. L. Lin, Chaos **16**, 037113 (2006).
[25] B. Marts and A. L. Lin, Phys. Rev. E **77**, 026211 (2008).
[26] S. Grill, V. S. Zykov, and S. C. Müller, Phys. Rev. Lett. **75**, 3368 (1995).
[27] M. Hildebrand, J. Cui, E. Mihaliuk, J. Wang, and K. Showalter, Phys. Rev. E **68**, 026205 (2003).
[28] S. Weiss and R. D. Deegan, Europhys. Lett. **110**, 60004 (2015).
[29] Q. Ouyang and H. L. Swinney, Chaos **1**, 411 (1991).
[30] Q. Ouyang and J.-M. Flesselles, Nature **379**, 143 (1996).
[31] R. J. Field, E. Koros, and R. M. Noyes, J. Am. Chem. Soc. **94**, 8649 (1972).
[32] R. J. Field and R. M. Noyes, J. Chem. Phys. **60**, 1877 (1974).
[33] H. J. Krug, L. Pohlmann, and L. Kuhnert, J. Phys. Chem. **94**, 4862 (1990).
[34] T. Amemiya, T. Ohmori, and T. Yamaguchi, J. Phys. Chem. A **104**, 336 (2000).
[35] M. C. Cross and P. C. Hohenberg, Rev. Mod. Phys. **65**, 851 (1993).